

# PbMg<sub>1/3</sub>Nb<sub>2/3</sub>O<sub>3</sub>/PbTiO<sub>3</sub> superlattices: An x-ray diffraction and Raman spectroscopy temperature-dependent study

H. Bouyanfif,<sup>1,\*</sup> N. Lemée,<sup>1,†</sup> M. El Marssi,<sup>1</sup> F. Le Marrec,<sup>1</sup> B. Dkhil,<sup>2</sup> J. Chevrel,<sup>2</sup> B. Fraisse,<sup>2</sup>  
J. C. Picot,<sup>1</sup> and M. G. Karkut<sup>1</sup>

<sup>1</sup>Laboratoire de Physique de la Matière Condensée, Université de Picardie Jules Verne, 33 rue Saint Leu, 80039 Amiens, France

<sup>2</sup>Laboratoire Structures, Propriétés et Modélisation des Solides, Ecole Centrale Paris, Grande Voie des Vignes,  
92295 Chatenay Malabry Cedex, France

(Received 14 March 2007; revised manuscript received 3 May 2007; published 31 July 2007)

We have used x-ray diffraction and Raman spectroscopy over a broad temperature range ( $90\text{ K} \leq T \leq 900\text{ K}$ ) to study the structural and dynamical behavior of  $[\text{PMN}_{(1-x)\Lambda}/(\text{PbTiO}_3)_{x\Lambda}]_{10}$  superlattices ( $x = 0.2, 0.5, 0.8$ ) (where PMN is  $\text{PbMg}_{1/3}\text{Nb}_{2/3}\text{O}_3$ ), which were epitaxially grown with a nominal wavelength  $\Lambda$  of  $130\text{ \AA}$  by pulsed laser deposition on MgO substrates buffered with  $\text{La}_{0.5}\text{Sr}_{0.5}\text{CoO}_3$ . We present a comparison of the results obtained on these superlattices with the temperature evolution of three fictitious superlattices constructed using the temperature-dependent data obtained on individual  $\text{PbTiO}_3$  and  $\text{PbMg}_{1/3}\text{Nb}_{2/3}\text{O}_3$  epitaxial thin films. From this study, we conclude that the PMN layers in superlattices retain the structural characteristics, including the tetragonal distortion, of relaxor thin films. The  $\text{PbTiO}_3$  layers exhibit in-plane polar orientation at all temperatures. X-ray diffraction shows the stabilization, due to biaxial stress, of the ferroelectric order up to at least  $873\text{ K}$  in the  $\text{PbTiO}_3$  layers ( $T_C = 763\text{ K}$  in bulk). The tetragonal symmetry and ferroelectric order of the  $\text{PbTiO}_3$  layers, as well as the relaxorlike behavior of the PMN layers, are confirmed by Raman spectroscopy.

DOI: [10.1103/PhysRevB.76.014124](https://doi.org/10.1103/PhysRevB.76.014124)

PACS number(s): 77.84.-s, 68.65.Cd, 78.30.-j, 61.10.Nz

## INTRODUCTION

We have recently published room temperature results on  $\text{PbMg}_{1/3}\text{Nb}_{2/3}\text{O}_3/\text{PbTiO}_3$  (PMN/PT) superlattices.<sup>1</sup> Associating ferroelectric oxides in superlattices is a potentially fruitful way to explore the possible coupling between ferroelectric materials and the impact they can produce on the physical properties due to the variations in superlattice (SL) nanoperiodicity and the concomitant changes in the strains felt by the constituent layers. With this aim, different systems have been studied combining a ferroelectric with a dielectric [ $\text{BaTiO}_3/\text{SrTiO}_3$  (Refs. 2–6) and  $\text{PbTiO}_3/\text{SrTiO}_3$  (Refs. 7 and 8)], with a paraelectric [ $\text{KNbO}_3/\text{KTaO}_3$  (Refs. 9 and 10)], or with a ferroelectric [ $\text{PbTiO}_3/\text{BaTiO}_3$  (Refs. 11 and 12)]. Improvement of ferroelectric or dielectric properties has been reported, such as an increase of the dielectric constant,<sup>2</sup> of the remanent polarization,<sup>2</sup> or of the Curie temperature<sup>9,12</sup> and are generally explained either by the intense strains induced in such structures<sup>2,9</sup> or by the domain-induced interlayer coupling in  $\text{KNbO}_3/\text{KTaO}_3$  superlattices.<sup>13</sup>

There is also an interest in associating a ferroelectric PT with the relaxor ferroelectric PMN. Indeed, the solid solution  $(1-x)\text{PbMg}_{1/3}\text{Nb}_{2/3}\text{O}_3-x\text{PbTiO}_3$  (PMN- $x$ PT) presents very attractive dielectric and piezoelectric performances suitable for transducer and actuator applications<sup>14</sup> which have motivated numerous studies on thin films for application in miniaturized devices.<sup>15–19</sup> Nevertheless, compared to the bulk, a decrease in the piezoelectric performances of the PMN- $x$ PT system is observed in thin films.<sup>15–19</sup> Strain, interfacial effects (dead layers), and defects have been invoked to explain this decrease of the physical performances compared to the bulk. The construction of PMN/PT superlattices might lead to a better understanding of such effects. Recent

results report on the possible presence of long-range coupling and strain in some nonepitaxial PMN/PT multilayers.<sup>20</sup> It would be of interest to know if the epitaxial strains induced in ferroelectric/relaxor SL layers could produce physical characteristics different from those of the constituents.

Recall that PT is a classical ferroelectric material which undergoes an abrupt first order transition at  $763\text{ K}$  from the high temperature paraelectric-cubic phase to the low temperature ferroelectric-tetragonal phase.<sup>21</sup> The stability of the PT ferroelectric phase in thin film form can be modified from that of the bulk by substrate-induced strains. Significant effort has been made to understand and predict the ferroelectric-ferroelastic domain structure observed in the PT thin films.<sup>22–24</sup> For the ferroelectric relaxor PMN, the dielectric response is characterized by a strong frequency dependence as a function of temperature.<sup>25</sup> The dielectric peak is not related to any phase transition and it is now widely admitted that the strong dispersion observed arises from the collective dynamic response of polar nanoregions. These polar nanoregions, embedded in a paraelectric matrix, appear at the so-called Burns temperature  $T_B = 600\text{ K}$ .<sup>26</sup> No ferroelectric phase transition takes place and PMN remains paraelectric down to  $5\text{ K}$ . Studies showing the effect of hydrostatic stresses on bulk PMN<sup>27,28</sup> and on thin films deposited on different substrates have been published.<sup>18</sup>

We have reported room temperature results on PMN/PT superlattices<sup>1</sup> of the type  $[\text{PMN}_{(1-x)\Lambda}/\text{PT}_{x\Lambda}]_{10}$ , where the periodicity  $\Lambda$  is approximately  $130\text{ \AA}$  and  $x$  is the ratio of PT in a period that varies from  $0.1$  to  $0.8$ . We have demonstrated by x-ray and Raman studies that the PT layers are entirely  $a$ -axis oriented along the growth direction, implying that the polarization  $c$  axis lies in the plane of the SL. In addition, in PT layers the stress can reach  $3.6\text{ GPa}$  and produces both a frequency decrease of the PT vibrational modes and a split-

TABLE I. Superlattice periodicities  $\Lambda$  and layer thicknesses in the period ( $t_{\text{PMN}}$  and  $t_{\text{PT}}$ ) estimated from  $\theta$ - $2\theta$  x-ray diffractograms reported in the Ref. 1.

	PMN <sub>(1-x)A</sub> /PT <sub>x</sub> A		
	$x=0.2$	$x=0.5$	$x=0.8$
Periodicity $\Lambda$ (Å)	130	150	150
$t_{\text{PMN}}$ (Å)	104	75	30
$t_{\text{PT}}$ (Å)	26	75	120

ting of the silent mode. Moreover, no stress dependence in the PMN layers was detected by the room temperature Raman spectra. Here, we report on the temperature-dependent x-ray and Raman response for three of these superlattices ( $x=0.2, 0.5, 0.8$ , see Table I). We choose to present these compositions since the trends that we have observed for them are representative of all the SL's we have studied as a function of temperature.

### EXPERIMENTAL PROCEDURE

The samples were grown by pulsed laser deposition using a Spectra Physik 248 nm laser in a MECA 2000 UHV chamber. A 1500 Å  $\text{La}_{0.5}\text{Sr}_{0.5}\text{CoO}_3$  (LSCO) electrode layer was deposited at a substrate temperature ( $T_s$ ) of 700 °C and 0.2 mbar oxygen partial pressure ( $P_{\text{O}_2}$ ). The oxygen pressure for PMN and PT layers was  $P_{\text{O}_2}=0.3$  mbar and the deposition temperatures were, respectively,  $T_s=545$  °C and  $T_s=600$  °C. The deposition rate (0.2 Å/pulse) was determined from the x-ray thickness oscillations observed on single films of PMN and of PT. The deposition system is equipped with a 15 kV reflection high-energy electron diffraction (RHEED) system, which enables us to monitor the surface quality of the layers. The x-ray measurements were performed using an in-house designed goniometer permitting high resolution measurements of the out-of-plane lattice parameter up to 600 °C. Raman measurements were performed using the 514.5 nm line from an argon ion laser and analyzed using a Jobin Yvon T64000 spectrometer equipped with a charge coupled device. An optical microscope was used to focus the incident light as a spot of about 0.5  $\mu\text{m}$  in diameter on the sample. Polarized Raman spectra have been recorded with respect to the crystallographic axes of  $a$ -domain PT layers ( $X\parallel[100]_{\text{MgO}}$ ,  $Y\parallel[001]_{\text{MgO}}$ , and  $Z\parallel[010]_{\text{MgO}}$ ). The temperature evolution from room temperature to 600 °C was measured using a Linkam hot stage. Electrical measurements carried out on the PMN film were made in capacitance geometry using the lower LSCO electrode initially grown and upper platinum electrodes 150  $\mu\text{m}$  in diameter prepared by standard photolithography and sputtering techniques. Dielectric constant and loss values were measured with a Schlumberger 1260 impedance meter in a Linkam modified stage, as a function of temperature (cooling from 383 to 113 K) and frequency (between 1 kHz and 1 MHz) at an excitation field of 0.8 kV/cm.

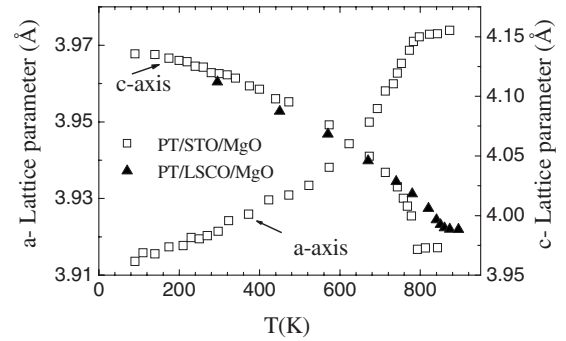


FIG. 1. Out-of-plane lattice parameters ( $a$  axis and  $c$  axis) vs temperature for a 2500 Å thick PT film deposited on MgO buffered with  $\text{SrTiO}_3$  (Ref. 31);  $c$ -axis lattice parameter vs  $T$  for a 1500 Å thick PT film deposited on MgO buffered with LSCO (Ref. 28). The  $T_C$ 's for these films are, respectively, 785 and 855 K.

### RESULTS AND DISCUSSION

As a prerequisite in interpreting the results that we have obtained on the PMN/PT superlattices, we have investigated the temperature behavior of individual PMN and PT thin films. Our previous RHEED and x-ray diffraction (XRD) studies on PMN thin films grown on (100) MgO substrates buffered with LSCO indicate that they are cube-on-cube epitaxial single phase films having no observable traces of pyrochlore. The temperature evolutions of the out-of-plane lattice parameter for the individual PT and PMN thin films are presented in Figs. 1 and 2, respectively. A more detailed study of these results can be found elsewhere.<sup>12,29-31</sup>

First of all, we present results on two different single PT thin films: one grown on MgO buffered with a layer of LSCO, and a second grown on MgO buffered with a thin layer of  $\text{SrTiO}_3$  (STO). Since structural studies of PT thin films have been well described previously,<sup>12,29</sup> we will only present the most important features. The lattice parameter of STO (3.905 Å) is extremely close to that of the  $a$  parameter of PT (3.899 Å), whereas the lattice parameter of LSCO (3.805 Å) is appreciably smaller than  $a_{\text{PT}}$  and thus should produce additional misfit strains in the films. The microstructure of the PT film deposited on LSCO/MgO is predominantly  $c$  oriented with only about 1%  $a$  orientation. The room temperature diffraction peaks related to the  $a$ -oriented domains are very weak—possibly due to the mismatch between film and buffer layer—and the extraction of  $a$ -axis values as a function of temperature was problematic and hence we present only the  $c(T)$  for this sample. Since PMN/PT SL's are  $a$  oriented, we need the PT film  $a$ -axis evolution to compare with the SL behavior; for this reason, we also present the second PT film grown on STO/MgO. This sample is also characterized by mixed  $c$ - and  $a$ -domain PT layers, but since this film consists of roughly 5%  $a$  domains, we were able to follow the evolution of the  $a$  axis up to the highest measuring temperature of 873 K. In Fig. 1, we present the temperature-dependent evolution of the lattice parameters for these two PT films.

The transition temperatures  $T_C$  determined from Fig. 1 are higher than that of the bulk  $T_C$  of PT (763 K). The  $T_C$  of the PT film grown on LSCO/MgO is about 70 K higher than the

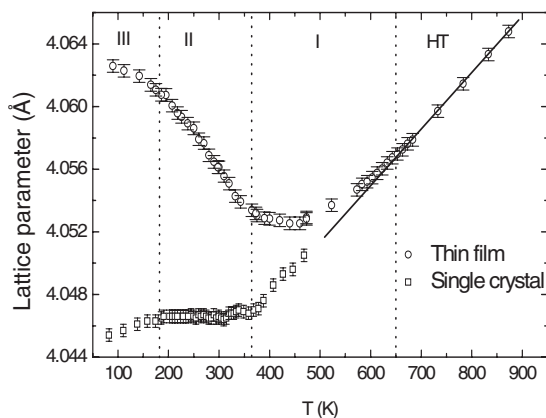


FIG. 2. Out-of-plane lattice parameter vs temperature for a PMN thin film and single crystal. The symbol  $\circ$  refers to the out-of-plane lattice parameter versus temperature for a 7000 Å thick PMN film (Ref. 29) deposited on MgO buffered with LSCO (1500 Å). The square symbols refer to the PMN single crystal data (Ref. 38). The solid line is a guide for the eye for the thin film data and evidences the change of slope at about 650 K (see text).

PT film grown on STO/MgO. This upward temperature shift evidences the influence of the buffer layer on the epitaxial strains in PT single films. This effect on the PT phase transition seems to be well understood. It has been the subject of previous experimental and theoretical studies,<sup>24,32–34</sup> which have established a clear relation between strain, domain structure, thickness and  $T_C$  of PT films grown on cubic substrates. In fact, the epitaxial strains in thin films—be they compressive or extensive—tend to stabilize the ferroelectric phase to higher temperatures. The  $T_C$  values are also strongly dependent on the domain structure. Indeed, the formation of  $c/a/c/a$  polydomain structures, such as those existing in the films presented in Fig. 1, enables a partial relaxation of stress<sup>35–37</sup> which cannot take place in purely  $c$ -oriented films. Consequently, the transition temperature in polydomain thin films will be lower than that in  $c$ -oriented films<sup>32</sup> and higher than that in stress-free bulk material.

We present in Fig. 2 the temperature-dependent out-of-plane lattice parameter of a PMN thin film along with the temperature evolution reported for bulk single crystal PMN. We designate four different temperatures zones (denoted I, II, III, and HT) which correspond to different trends in the lattice parameter variation for *both* the thin film and the single crystal. The high temperature (HT) zone corresponds to temperatures greater than 650 K for which the lattice parameter is linear in temperature. The onset of zone I occurs at about 650 K (this is commonly called the Burns temperature) where we observe a deviation from linearity of the thin film lattice parameter. In the bulk, the Burns temperature corresponds to the nucleation of polar nanoregions. From 470 to 370 K the film parameter remains constant in contrast to the continuously decreasing parameter of the single crystal. As the PMN enters zone II, around 370 K, the thin film lattice parameter exhibits a negative thermal expansion coefficient, whereas in the bulk it is close to zero. In the bulk, XRD, Raman spectroscopy, acoustic emission, and dielectric permittivity<sup>38–41</sup> studies have demonstrated the correlation

between this anomaly and the beginning of the relaxor phenomena due to the growth of polar nanoregions. These studies also indicate the presence of local phase transitions and the increase of the polar correlation length with decreasing temperature. Finally, in zone III, below 200 K the film lattice parameter increases less rapidly, while the bulk parameter begins to slowly decrease. The temperature of 200 K is linked to the so-called freezing temperature of the polar nanoregions.

The differences in the temperature-dependent evolution of the bulk and thin film lattice parameters can be explained by the thermal misfit between the substrate and the PMN layer which produces an in-plane compressive thermal stress, the result of which is to increase the out-of-plane lattice parameter observed in the experimental data. This effect is most evident in zone II where the thermal expansion coefficient of MgO ( $\alpha \sim 8$  ppm K<sup>-1</sup> for  $T < 300$  K and 13 ppm K<sup>-1</sup> for  $T > 300$  K) is significantly larger than that of the PMN layer ( $\alpha_{\text{bulk}} < 1$  ppm K<sup>-1</sup>). This results in the observed tetragonal distortion at room temperature  $d_{\perp}/d_{\parallel} = 1.001$  which increases to 1.004 at 90 K.<sup>30</sup>

Complementing these x-ray measurements, we have used Raman spectroscopy which is very sensitive to the polar nature of materials. The Raman signal for the pseudocubic bulk single crystal of PMN is explained by the local deviation of the cubic symmetry due to intrinsic disorder, the polar nanoregions, and/or the presence of chemically ordered nanoregions. We measured the Raman spectra of a PMN 1500 Å thick film at different temperatures in order to verify if such a tetragonal structural distortion could have induced change from a relaxor to a ferroelectric phase. This sample was selected since it is characterized by a  $d_{\perp}/d_{\parallel}$  value (1.008 at 90 K) that is larger than that of the PMN 7000 Å thick film, and therefore the impact of the tetragonal distortion is expected to be more obvious. Figure 3 presents the temperature dependence between 110 and 773 K of the polarized Raman spectra recorded in  $Y(XX)\bar{Y}$  and  $Y(XZ)\bar{Y}$  scattering geometries.

As with bulk PMN single crystal,<sup>42</sup> the thin film Raman spectra are polarized for the whole range of temperature investigated. The polarization dependent Raman spectra demonstrate the epitaxial nature of the thin film. Apart from an expected decrease of the Raman intensity and a broadening of the Raman modes, we do not observe a significant modification of the thin film Raman spectra compared to that of the bulk single crystal. The Raman modes of the thin film occur at the same frequencies as that of the bulk and we do not detect any change as a function of temperature. This fact indicates, at least, the absence of a transition toward a rhombohedral ferroelectric phase as has been observed in single crystal PMN-PT upon application of an electric field. This is particularly clear on viewing the ratio of the polarization dependence of the high frequency mode at 780 cm<sup>-1</sup>: the parallel polarization line is much more intense than that of the crossed polarization line and their ratio remains essentially constant over the entire temperature range. This is in contrast to the abrupt change in the depolarization ratio of this mode which has been used to determine the onset of the rhombohedral ferroelectric phase under field and at low temperature in PMN related systems.<sup>42</sup>

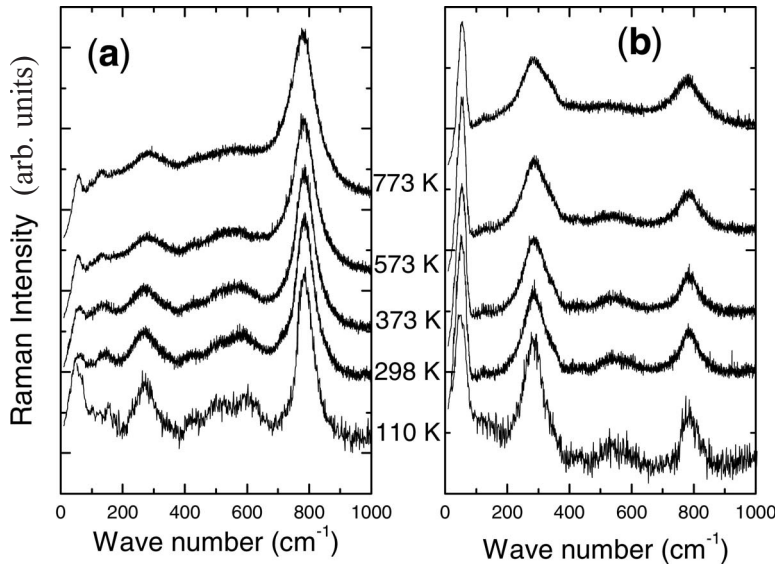


FIG. 3. Temperature-dependent Raman spectra of a 1500 Å PMN thick film in (a) parallel polarization  $Y(XX)\bar{Y}$  and (b) crossed polarization  $Y(XZ)\bar{Y}$ .

While the PMN bulk Raman spectra are sensitive to hydrostatic pressure,<sup>27,28</sup> no frequency shift in the Raman modes is observed in our strained PMN thin film. This can be explained by the different nature of the stress—two dimensional versus three dimensional—or by a smaller magnitude of the stress in the thin film (a few gigapascals) compared to that usually applied in hydrostatic pressure studies (more than 3.5 GPa) before significant change in Raman spectra takes place.<sup>28</sup> Despite the tetragonal distortion of the thin film observed by XRD, the Raman study indicates no change in symmetry and in the polar state on the local range in the PMN thin films. If there would have been a strain induced ferroelectric phase, the Raman measurements would have enabled us to detect this transition. Of course, Raman spectroscopy alone cannot confirm relaxor behavior, it can only suggest it. Therefore, we have complemented this study with dielectric measurements.

The dielectric constant and the loss tangent are plotted as a function of temperature for different frequencies in Fig. 4 for a 2500 Å thick PMN film. The diffuse  $\epsilon(T)$  response and the shift to higher temperatures with increasing frequency of the permittivity maxima, along with an increase of the dielectric loss and a shift toward higher temperature of the maximum, are characteristics of relaxor behavior. These electrical measurements clearly demonstrate the persistence of relaxor behavior despite the tetragonal distortion in the film, and reinforce our interpretation, suggested by the temperature-dependent evolution of the lattice parameter and the Raman spectra, that this film is a relaxor. However, compared with bulk ceramics (16 000 at 10 kHz), the maximum permittivity is low (800 at 10 kHz) but it is comparable with values already reported on thin films.<sup>17,43</sup> Moreover, contrary to the bulk, and as already observed in PMN films,<sup>17</sup> the dielectric behavior of the film exhibits frequency dispersion immediately above  $T_m$ . To explain these differences, several mechanisms are often invoked such as the influence of the interfacial layers and of the presence of dislocations and oxygen vacancies. In addition, the tetragonal distortion can also be a contributing factor to the dispersion in the dielectric response of the polar nanoregions.

We now turn to the  $\text{PMN}_{(1-x)\Lambda}/\text{PT}_{x\Lambda}$  superlattices. The RHEED streaks we observe from the PMN and PT layers indicate cube-on-cube epitaxial growth.<sup>31</sup> In SL's, the diffraction conditions are given by  $n_{\text{sat}}\lambda = 2\Lambda \sin(\theta_{n_{\text{sat}}})$ , where  $n_{\text{sat}}$  corresponds to the superlattice diffraction order,  $\lambda$  the x-ray wavelength,  $\theta_{n_{\text{sat}}}$  is the angular position of the satellite peaks, and  $\Lambda = N_{\text{PT}}d_{\text{PT}} + N_{\text{PMN}}d_{\text{PMN}}$  is the modulation wavelength with  $N_{\text{PT}}$  ( $N_{\text{PMN}}$ ) the number of unit cell and  $d_{\text{PT}}$  ( $d_{\text{PMN}}$ ) is the unit cell parameter along the growth direction of the PT layers (PMN layers). The room temperature diffractograms of the  $\text{PMN}_{(1-x)\Lambda}/\text{PT}_{x\Lambda}$  superlattices have already been presented in Ref. 1. These diffractograms exhibit equally spaced satellite peaks which are characteristic of the chemical modulation imposed along the growth direction. To investigate the temperature-dependent structural variations of the SL's, we have followed the temperature evolution of the  $\theta$ - $2\theta$  XRD patterns obtained on three different SL samples. Figure 5 displays the temperature evolution of the average lattice parameter  $a_{\text{SL}} = \Lambda/n_{\text{sat}}$  [ $=\lambda/2 \sin(\theta_{n_{\text{sat}}})$ ] between 100

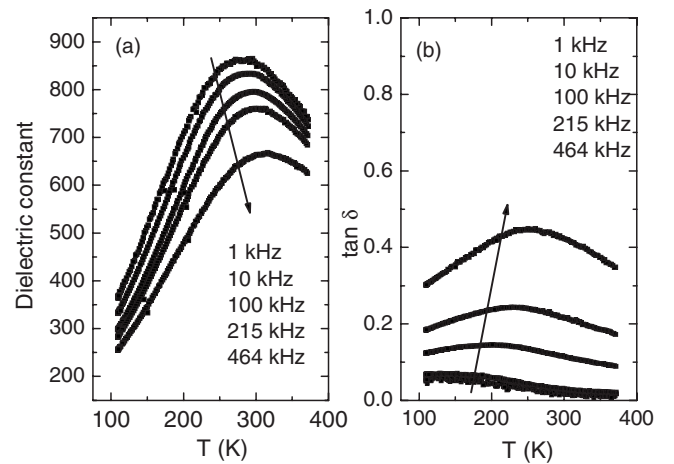


FIG. 4. Evolution with temperature and frequency of (a) the dielectric constant and (b) the dielectric loss of a 2500 Å PMN thin film deposited on MgO buffered with LSCO electrode. Arrows indicate increasing frequency.

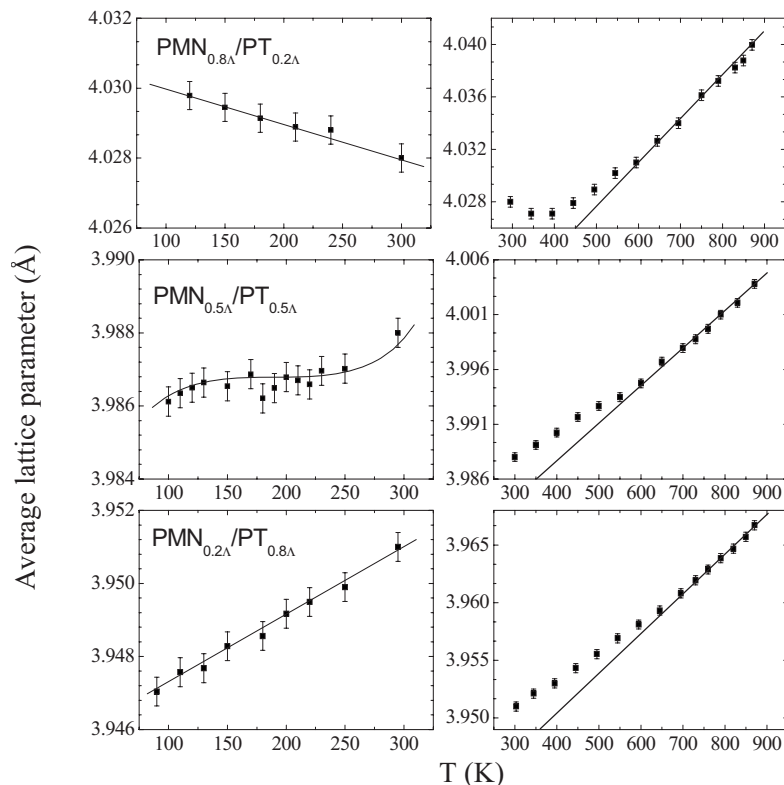


FIG. 5. Evolution with temperature of the average lattice parameter for the superlattices  $\text{PMN}_{(1-x)\Lambda}/\text{PT}_{x\Lambda}$  with  $x=0.8, 0.5,$  and  $0.2$ . Since the variations of the lattice parameters differ by about a factor of 5 between the low and high temperature ranges, we separate, for the sake of clarity, these two regions with the data point at 300 K common to both. Guides for the eyes are used for the low temperature side. The solid lines at high temperature highlight a change in slope in the evolution.

and 873 K. The change with temperature of this average lattice parameter is a result of the combined evolution of the out-of-plane lattice parameter of each constituent in the superlattices.<sup>11</sup> If any structural anomalies occur in the PMN and/or PT layers of the superlattices, the average lattice parameters  $a_{\text{SL}}$  should reflect it.

What is evident for all three samples is that at high temperatures ( $300 \text{ K} \leq T \leq 873 \text{ K}$ ), the lattice parameter is linear in temperature with a deviation from linearity occurring at roughly 600 K. At lower temperatures ( $80 \text{ K} \leq T \leq 300 \text{ K}$ ), the parameter either increases, saturates, or decreases on cooling depending on the ratio of PT in the SL wavelength. To better understand this temperature behavior and to compare it with the thin films, we have created three fictitious superlattices having the same superlattice wavelength  $\Lambda$  and the same ratio of PMN to PT as the SL samples presented above. We have calculated an average fictitious lattice parameter by using the temperature dependence of the lattice parameters of the single thin film of PT grown on STO/MgO presented in Fig. 1 and of PMN grown on LSCO/MgO of Fig. 2. For the former, we use the  $a$ -axis values (nonpolar axis) which correspond to the orientation of PT in these SL's. These fictitious SL's are comparable to a noninteractive stacking of individual PMN and PT layers grown on MgO, and so any coupling between the layers in the real SL samples might show up as differences between the diffractograms of the experimental and fictitious SL's. We are, of course, aware that we have to be cautious in comparing these SL's: a quantitative comparison is problematic since the strain fields that exist in the simulated SL's will reflect those of the single thin films of PMN and PT, whereas the strains in a real SL structure is expected to be more intense. This is

so because the layers of the SL experience strains produced by the mismatch with the adjacent (top and bottom) constituent layers. Even so, we are still able to make some general observations concerning the SL behavior.

For each temperature, the fictive average lattice parameter is given by  $a_{\text{ave}} = [N_{\text{PMN}}d_{\text{PMN}}(T) + N_{\text{PT}}d_{\text{PT}}(T)]/n_{\text{sat}}$ ,  $d_{\text{PT}}(T)$  and  $d_{\text{PMN}}(T)$  correspond, respectively, to the  $a$ -axis evolution depicted in Fig. 1 and to the out-of-plane lattice parameters of Fig. 2.  $n_{\text{sat}}$  corresponds to the order of diffraction for the most intense satellite peak and is also equal to  $(N_{\text{PMN}} + N_{\text{PT}})$ , which renders our definition of  $a_{\text{ave}}$  equivalent to that in Ref. 8. The results obtained using this procedure are presented in Fig. 6 for three superlattices  $\text{PMN}_{(1-x)\Lambda}/\text{PT}_{x\Lambda}$  with  $x=0.8, 0.5,$  and  $0.2$ .

At low temperatures ( $T < 300 \text{ K}$ ), we see that the results of Fig. 6 reproduce qualitatively the behavior of the Fig. 5 SL samples. In both Figs. 5 and 6, the temperature evolution depends on the ratio of PMN to PT in the modulation period. The change in slope of the temperature dependence of the lattice parameters reflects the ratio between the relaxor and the ferroelectric in the SL wavelength: it is negative for the PMN rich SL, constant for the 50/50 SL, and positive for the PT rich SL. On the high temperature side, the simulated out-of-plane lattice parameter increases smoothly from about 350 to 700 K, in agreement with the measured values of the SL samples in this temperature range. This is independent of the PMN/PT ratio. However, above 700 K and up to 873 K, the highest measuring temperature, the behavior of the three fictitious SL's diverges from that of their real counterparts. The anomalies evident in Fig. 6 above 780 K for the three simulated superlattices are not observed in the experimental data reported in Fig. 5 for the SL samples. These anomalies

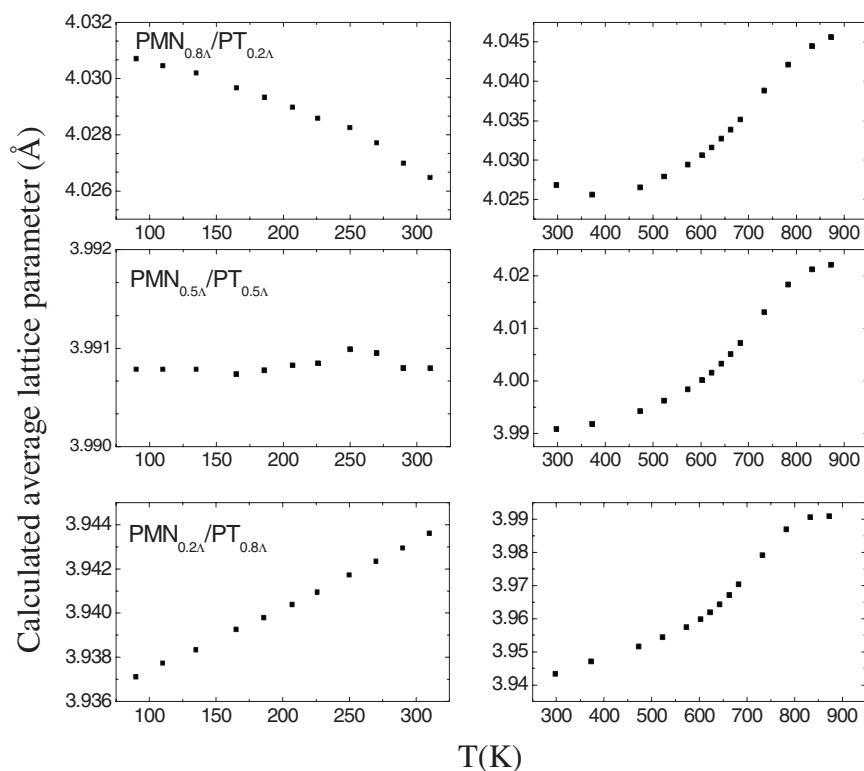


FIG. 6. The average lattice parameter evolution with temperature for three simulated superlattices  $\text{PMN}_{(1-x)\Lambda}/\text{PT}_{x\Lambda}$  with  $x = 0.8, 0.5,$  and  $0.2$ , calculated from the behavior of a PMN and a PT thin film (see text).

in the fictitious SL's correspond to the ferroelectric structural phase transition that takes place in the PT film grown on MgO buffered with STO seen in Fig. 1. The linear continuation of the experimentally determined lattice parameters up to 873 K in Fig. 5 strongly suggests the stabilization of the ferroelectric phase in the PT layers of these three SL's. Moreover, no change is observed in the full width at half maximum of the diffraction peaks of the SL samples; this is additional evidence that no structural phase transition is taking place in these SL's at these temperatures.

The absence of a phase transition (or equivalently the stabilization of the polar phase) indicates that the SL strains are clearly more significant than those that exist in the single PT thin films grown on buffered MgO shown in Fig. 1. This suggests that even if the origin and nature of the strains occurring in the superlattices are dissimilar to the asymmetric strain profile occurring in single thin films on single crystal substrates, the overall effect on the ferroelectric behavior is similar: strains stabilize the tetragonal structure. The ferroelectric phase stabilization by these means in PT has been previously reported in PT/BT superlattices.<sup>12</sup>

For the three SL's shown in Fig. 5, we observe a deviation from linearity which is composition dependent. This nonlinear onset occurs at 590 K for the  $\text{PMN}_{0.8\Lambda}/\text{PT}_{0.2\Lambda}$  sample and increases to about 650 K in the  $\text{PMN}_{0.2\Lambda}/\text{PT}_{0.8\Lambda}$  SL. We do not observe this variation for the corresponding fictitious superlattices since the nonlinear onset takes place at about the same temperature—650 K—for both the PT and the PMN thin films as can be seen in Figs. 1 and 2. In PMN thin films, this nonlinearity is due to the appearance of the polar nanoregions and was first observed as a change in the index of refraction by Burns and Dacol.<sup>26</sup> However, in PT thin films, the PT  $a$  axis is also intrinsically nonlinear in this

same temperature region (see Fig. 1). Thus, the temperature dependence of the nonlinear onset that we observe in the superlattices is probably a combined effect due to the relaxor and the ferroelectric layers. From 550 down to 90 K, the behavior of the SL samples is clearly very similar to the fictitious ones. This comparison suggests that the tetragonal distortion observed in the PMN single films is also present in the SL PMN layers, and that no major change has occurred in the PMN relaxor behavior compared with the PMN single films. Indeed, it is possible to explain the structural behavior of the superlattices from the PMN and PT thin films by assuming that the in-plane stress interactions between the SL layers are strong enough to stabilize the ferroelectric phase at higher temperatures but too weak to induce observable changes in the relaxor behavior. The impact of pressure on relaxor characteristics is thoroughly treated by Samara in a review article,<sup>27</sup> and recent structural and polar instabilities in bulk PMN have been reported in a high pressure investigation by Raman spectroscopy.<sup>28</sup> The pressure values required to observe such modifications are very important (at least 5.5 GPa) and obviously higher than the ones reached in our SL's, which we have estimated<sup>1</sup> to be on the order of 2.5 GPa in the PT layers. This estimation is calculated from the linear decrease of the soft-mode frequency with increasing pressure up to 12 GPa reported in the papers by Sanjujo *et al.*<sup>44</sup> and Cerdeira *et al.*<sup>45</sup>

To further confirm the ferroelectric phase stabilization of PT in these PMN/PT SL's, we used Raman spectroscopy to study the temperature dependence of the vibrational modes of a  $\text{PMN}_{0.5\Lambda}/\text{PT}_{0.5\Lambda}$  superlattice. Following the temperature evolution of the soft modes is a well established method for observing structural phase transitions. Studies on PT bulk single crystals have shown that Raman selection rules are

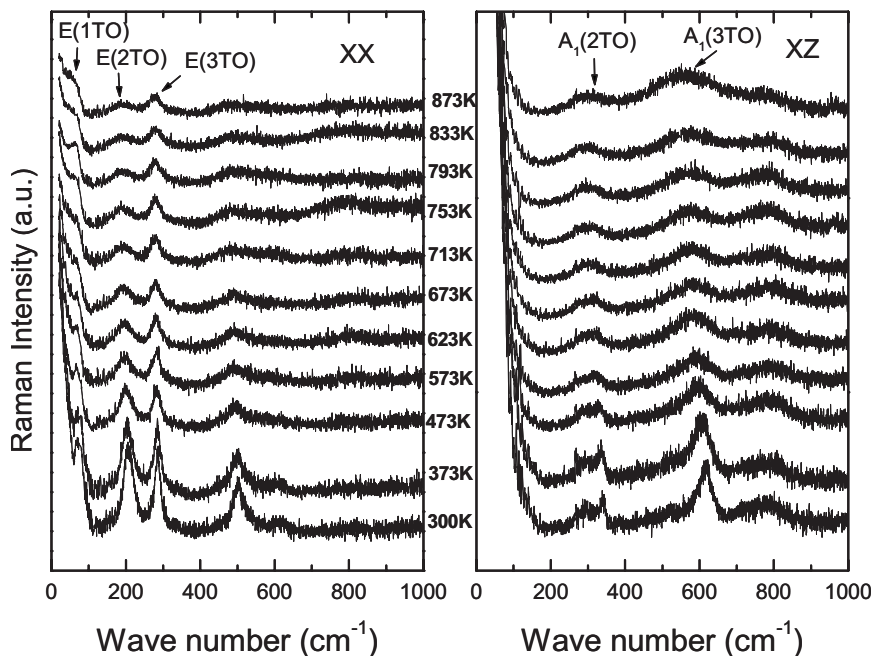


FIG. 7. Raman spectra of the superlattice PMN<sub>0.5Λ</sub>/PT<sub>0.5Λ</sub> between 300 and 873 K recorded in parallel polarization  $Y(XX)\bar{Y}$  and crossed polarization  $Y(XZ)\bar{Y}$  configurations.

strictly obeyed for both the ferroelectric and paraelectric phases,<sup>21,46,47</sup> and in the bulk the sudden disappearance of the soft mode with increasing temperature signals the transition from the ferro- to the paraelectric phase.<sup>21</sup> In some thin films, the soft mode does not disappear but saturates due to the strain field distribution produced by the substrate.<sup>48</sup> Figure 7 shows the Raman spectra recorded in the  $Y(XX)\bar{Y}$  and  $Y(XZ)\bar{Y}$  geometries between 300 and 873 K. We have previously performed a room temperature study on these SL's and have attributed the presence of certain Raman normal modes to be consistent with an *a*-axis orientation in the PT layers.<sup>1</sup> This is of course in agreement with our XRD results and analysis for these same samples. As for the bulk, the mode frequencies decrease with temperature, whereas their widths increase with temperature. This is clearly evident in Fig. 7 for the polar modes  $E(1TO)$ ,  $E(2TO)$ , and  $A_1(3TO)$ . However, contrary to the bulk, the evolution of the Raman spectra is gradual and no abrupt changes occur at any temperature. We observe a persistence of all the polar modes characteristic of the ferroelectric order up to 873 K. The Raman spectra in crossed and parallel configurations remain distinct and the soft  $E(1TO)$  mode is clearly discernible at the highest measured temperatures.

Figure 8 displays the temperature dependence of the  $E(1TO)$  soft-mode frequency, which has previously been used to study the stress in PT films<sup>48</sup> and in PT layers in PT-based SL's.<sup>12</sup> The low-frequency band of the XZ spectra was fitted using three peaks: two PMN modes at 47 and 62 cm<sup>-1</sup> and one PT  $E(1TO)$  mode (see Ref. 1 for a detailed explanation). Data recorded on a PT single crystal<sup>48</sup> are also indicated for comparison. The SL data are discontinued at 773 K since above this temperature it was impossible to extract the soft-mode frequency because of the increasingly strong overlap of the PT and the PMN modes. Between 300 and 600 K, the soft-mode SL frequency is lower than the frequencies of the PT single crystal. This is due to the strains

in the SL. Above 600 K, the variation of the soft-mode frequency is less pronounced compared to that of the single crystal. In the single crystal, a decrease of the soft-mode frequency is observed from 89 to 52 cm<sup>-1</sup> and is followed by an abrupt disappearance of this mode at the structural phase transition. In contrast, the superlattice soft-mode behavior clearly indicates the stabilization of the ferroelectric phase (i.e.,  $T_C$  is shifted to higher temperature) in the PT layers of the PMN<sub>0.5Λ</sub>/PT<sub>0.5Λ</sub> superlattice and thus confirms the x-ray interpretation of a strain induced increase of  $T_C$ . This result is consistent with the influence of strain on the PT single thin film ferroelectric transition presented in Fig. 1 and with the reduction of the soft-mode frequency of a PT single thin film reported in Ref. 12.

In summary, we have studied the temperature-dependent behavior of three superlattices [PMN<sub>(1-x)Λ</sub>/PT<sub>xΛ</sub>]<sub>10</sub> ( $x=0.2, 0.5,$  and  $0.8$ ) by x-ray diffraction and modeling and by Raman spectroscopy. We have compared the results with the

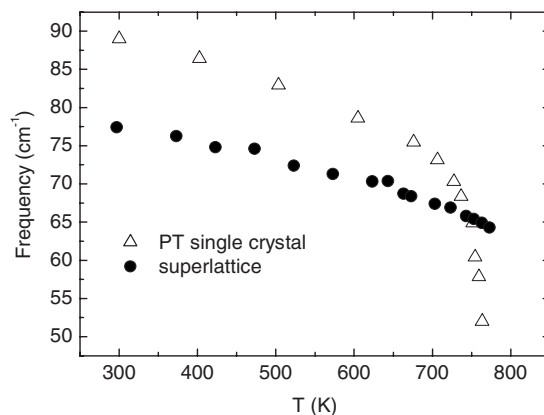


FIG. 8. Evolution of the frequency of the soft mode  $E(1TO)$  as a function of temperature for a superlattice PMN<sub>0.5Λ</sub>/PT<sub>0.5Λ</sub> and a PT single crystal (Refs. 21 and 48).

data recorded on individual PMN and PT thin films. In these artificial superlattice structures, the strain effect on PMN and PT layers changes with composition. We provide evidence that the in-plane strain generated by these structures (estimation of stress around 2.5 GPa in PT layers) stabilizes the ferroelectric phase up to at least 873 K in the PT layers which is 100 K greater than the  $T_C$  of bulk PT. In the PMN layers of these SL's, the stress induces a tetragonal distortion which is not strong enough to provide a detectable impact on the relaxorlike structural behavior. Electrical measurements

are now under way to provide additional information on the relaxor character of the PMN layers in these superlattices.

#### ACKNOWLEDGMENTS

We thank Eric Cattan for assistance with the electrical measurements. We are grateful to the Region of Picardie for financial support. This work was partially supported by an E.U. STREP MULTICERAL (Contract No. FP-6-NMP-CT-2006-032616).

- 
- \*Present address: Group of Solid State Physics, Department of Physics, University of Fribourg, 3 Ch. Du Musée, 1700 Fribourg, Switzerland.
- <sup>†</sup>Author to whom correspondence should be addressed; nathalie.lemee@sc.u-picardie.fr
- <sup>1</sup>H. Bouyanfif, M. El Marssi, N. Lemée, F. Le Marrec, M. G. Karkut, and B. Dkhil, *Phys. Rev. B* **71**, 020103(R) (2005).
- <sup>2</sup>H. Tabata, H. Tanaka, and T. Kawai, *Appl. Phys. Lett.* **65**, 1970 (1994).
- <sup>3</sup>T. Shimuta, O. Nakagawara, T. Makino, S. Arai, H. Tabata, and T. Kawai, *J. Appl. Phys.* **91**, 2290 (2002).
- <sup>4</sup>K. Johnston, X. Huang, J. B. Neaton, and K. M. Rabe, *Phys. Rev. B* **71**, 100103(R) (2005).
- <sup>5</sup>A. A. Q. Jiang, J. F. Scott, Huibin Lu, and Zhenghao Chen, *J. Appl. Phys.* **93**, 1180 (2003).
- <sup>6</sup>Rasmi R. Das, Yu. I. Yuzyuk, P. Bhattacharya, V. Gupta, and R. S. Katiyar, *Phys. Rev. B* **69**, 132302 (2004).
- <sup>7</sup>J. C. Jiang, X. Q. Pan, W. Tian, J. C. D. Theis, and D. G. Schlom, *Appl. Phys. Lett.* **74**, 2851 (1999).
- <sup>8</sup>M. Dawber, C. Lichtensteiger, M. Cantoni, M. Veithen, P. Ghosez, K. Johnston, K. M. Rabe, and J. M. Triscone, *Phys. Rev. Lett.* **95**, 177601 (2005).
- <sup>9</sup>H.-M. Christen, E. D. Specht, D. P. Norton, M. F. Chisolm, and L. A. Boatner, *Appl. Phys. Lett.* **72**, 2535 (1998).
- <sup>10</sup>J. Sigman, D. P. Norton, H. M. Christen, P. H. Fleming, and L. A. Boatner, *Phys. Rev. Lett.* **88**, 097601 (2002).
- <sup>11</sup>F. Le Marrec, R. Farhi, M. El Marssi, J.-L. Dellis, M. G. Karkut, and D. Ariosa, *Phys. Rev. B* **61**, R6447 (2000).
- <sup>12</sup>F. Le Marrec, R. Farhi, B. Dkhil, J. Chevreul, and M. G. Karkut, *J. Eur. Ceram. Soc.* **21**, 1615 (2001).
- <sup>13</sup>V. A. Stephanovich, I. A. Lukyanchuk, and M. G. Karkut, *Phys. Rev. Lett.* **94**, 047601 (2005).
- <sup>14</sup>S. Park and T. R. ShROUT, *J. Appl. Phys.* **82**, 1804 (1997).
- <sup>15</sup>D. Lavric, R. A. Rao, Q. Gan, J. J. Krajewski, and C. B. Eom, *Integr. Ferroelectr.* **21**, 499 (1998).
- <sup>16</sup>M. Tyunina and J. Levoska, *Phys. Rev. B* **63**, 224102 (2001); **65**, 132101 (2002).
- <sup>17</sup>G. Catalan, M. H. Corbett, R. M. Bowman, and J. M. Gregg, *Appl. Phys. Lett.* **74**, 3035 (1999); *J. Appl. Phys.* **91**, 2295 (2002).
- <sup>18</sup>V. Nagarajan, S. P. Alpay, C. S. Ganpule, B. K. Nagaraj, S. Agarwal, E. D. Williams, A. L. Roytburd, and R. Ramesh, *Appl. Phys. Lett.* **77**, 438 (2000).
- <sup>19</sup>J. H. Park, F. Xu, and S. Trolrier-McKinstry, *J. Appl. Phys.* **89**, 568 (2000).
- <sup>20</sup>R. Ranjith, R. Nikhil, and S. B. Krupanidhi, *Phys. Rev. B* **74**, 184104 (2006).
- <sup>21</sup>G. Burns and B. A. Scott, *Phys. Rev. B* **7**, 3088 (1973).
- <sup>22</sup>C. M. Foster, Z. Li, M. Buckett, D. Miller, P. M. Baldo, L. E. Rehn, G. R. Bai, D. Guo, H. You, and K. L. Merkle, *J. Appl. Phys.* **78**, 2607 (1995).
- <sup>23</sup>V. G. Koukhar, N. A. Pertsev, and R. Waser, *Phys. Rev. B* **64**, 214103 (2001).
- <sup>24</sup>K. S. Lee, J. H. Choi, J. Y. Lee, and S. Baik, *J. Appl. Phys.* **90**, 4095 (2001).
- <sup>25</sup>L. E. Cross, *Ferroelectrics* **76**, 241 (1987).
- <sup>26</sup>G. Burns and F. H. Dacol, *Solid State Commun.* **48**, 853 (1983).
- <sup>27</sup>G. A. Samara, *Solid State Phys.* **56**, 239 (2001), and references therein.
- <sup>28</sup>J. Kreisel, B. Dkhil, P. Bouvier, and J.-M. Kiat, *Phys. Rev. B* **65**, 172101 (2002).
- <sup>29</sup>H. Bouyanfif, Ph.D. thesis, University of Picardie, Amiens, France, 2005; (unpublished).
- <sup>30</sup>N. Lemée, H. Bouyanfif, F. Le Marrec, M. G. Karkut, B. Dkhil, J. Chevreul, and J.-M. Kiat, *Ferroelectrics* **288**, 277 (2003).
- <sup>31</sup>H. Bouyanfif, N. Lemée, M. El Marssi, F. Le Marrec, B. Dkhil, and M. G. Karkut, *Ferroelectrics* **316**, 1 (2005).
- <sup>32</sup>S. K. Streiffer, J. A. Eastman, D. D. Fong, C. Thompson, A. Munkholm, M. V. Ramana Murty, O. Auciello, G. R. Bai, and G. B. Stephenson, *Phys. Rev. Lett.* **89**, 067601 (2002).
- <sup>33</sup>D. Fong, G. Brian Stephenson, S. K. Streiffer, J. A. Eastman, O. Auciello, P. H. Fuoss, and C. Thompson, *Science* **304**, 1650 (2004).
- <sup>34</sup>D. D. Fong, A. M. Kolpak, J. A. Eastman, S. K. Streiffer, P. H. Fuoss, G. B. Stephenson, C. Thompson, D. M. Kim, K. J. Choi, C. B. Eom, I. Grinberg, and A. M. Rappe, *Phys. Rev. Lett.* **96**, 127601 (2006).
- <sup>35</sup>A. L. Roytburd, *Phys. Status Solidi A* **37**, 329 (1976).
- <sup>36</sup>J. S. Speck and W. Pompe, *J. Appl. Phys.* **76**, 466 (1994).
- <sup>37</sup>S. P. Alpay and A. L. Roytburd, *J. Appl. Phys.* **83**, 4714 (1998).
- <sup>38</sup>For a detailed description of the bulk structural behavior see, for example, B. Dkhil, Ph.D. thesis, Université of Paris XI Orsay, Paris, France 1999, and B. Dkhil, J.-M. Kiat, G. Calvarin, G. Baldinozzi, S. B. Vakrushev, and E. Suard, *Phys. Rev. B* **65**, 024104 (2002).
- <sup>39</sup>O. Svitelskiy, J. Toulouse, G. Yong, and Z.-G. Ye, *Phys. Rev. B* **68**, 104107 (2003).
- <sup>40</sup>E. Dul'kin, M. Roth, B. Dkhil, and J. M. Kiat, *J. Appl. Phys.* **98**, 023520 (2005).
- <sup>41</sup>C. Elissalde, Ph.D. thesis, Université of Bordeaux I, Bordeaux, France, 1994.

- <sup>42</sup>M. El Marssi, R. Farhi, and Y. I. Yuzyuk, *J. Phys.: Condens. Matter* **10**, 9161 (1998).
- <sup>43</sup>G. R. Bai, S. K. Streiffer, P. K. Baumann, O. Auciello, K. Ghosh, S. Stemmer, A. Munkholm, C. Thompson, R. A. Rao, and C. B. Eom, *Appl. Phys. Lett.* **76**, 3106 (2000).
- <sup>44</sup>J. A. Sanjurjo, E. Lopez-Cruz, and G. Burns, *Phys. Rev. B* **28**, 7260 (1983).
- <sup>45</sup>F. Cerdeira, W. B. Holzapfel, and D. Bäuerle, *Phys. Rev. B* **11**, 1188 (1975).
- <sup>46</sup>G. Burns and B. A. Scott, *Phys. Rev. Lett.* **25**, 167 (1970).
- <sup>47</sup>C. M. Foster, Z. Li, M. Grimsditch, S. K. Chan, and D. J. Lam, *Phys. Rev. B* **48**, 10160 (1993).
- <sup>48</sup>Y. I. Yuzyuk, R. Fahri, V. Lorman, L. M. Rabkin, L. A. Sapozhnikov, E. V. Sviridov, and I. N. Zakharchenko, *J. Appl. Phys.* **84**, 452 (1998).